Chemical Science

EDGE ARTICLE

View Article Online
View Journal | View Issue

Cite this: *Chem. Sci.*, 2019, **10**, 3257

All publication charges for this article have been paid for by the Royal Society of Chemistry

B- and N-embedded color-tunable phosphorescent iridium complexes and B–N Lewis adducts with intriguing structural and optical changes†

Qiuxia Li,[a] Chao Shi, *[ab] Manli Huang,[c] Xing Wei,[d] Hong Yan, *[d] Chuluo Yang *[c] and Aihua Yuan *[ab]

Received 25th September 2018
Accepted 17th January 2019

DOI: 10.1039/c8sc04252g

rsc.li/chemical-science

A novel family of B- and N-embedded phosphorescent iridium complexes has been prepared. Single crystal structures indicate that the B-embedded polycyclic unit exhibits better planarity than the N-embedded polycyclic unit, which leads to different π–π-stacking and electrical characteristics. More importantly, by controlling the number of boron or nitrogen atoms embedded, solution-processed OLED devices incorporating these emitters as emitting layers can achieve a phosphorescence color variation from green to deep red (638 nm) and show low-efficiency roll-off and turn-on voltage. In particular, the B-embedded complex Ir-BB shows good color purity with a narrow full width at half maximum (1211 cm^{-1}) and CIE coordinates (0.67, 0.31) in the deep red light region. Notably, B-embedded iridium complexes can also react with two different Lewis bases (pyridine and DMAP) to form intriguing B–N Lewis adducts through different coordination modes. During this process, significantly different structural and optical changes are triggered by the structure and electronic properties of Lewis bases, as confirmed by X-ray crystallographic, ^{1}H NMR and spectral analysis.

Introduction

Boron (B) or nitrogen (N) atom-embedded planar π-conjugated organic semiconductors[1–16] have attracted much attention due to intriguing structural and electronic features, which are very promising in the fields of organic solid luminescent materials, magnetic materials, two-photon materials, carrier-transporting materials and chemosensors. Recently, a limited number of reports appeared on B- and N-embedded dioxygen-bridged polycyclic unit-based small organic molecules,[15,16] which were used as host materials in phosphorescent organic light-emitting diodes (OLEDs) and hole-transporting materials in organic field-effect transistors (OFETs). However, little attention has been paid to tuning photophysical properties of phosphorescent metal complexes by the use of B- or N-embedded polycyclic units. More importantly, how the rigidity, planarity and electronic effects of these units affect the structure, carrier transport and luminescence of metal complexes is well worth studying.

On the other hand, phosphorescent iridium(III) complexes[17–29] have attracted a great deal of interest as emitting materials owing to their rich and diverse chemical structures, high luminescence efficiency, appropriate phosphorescence lifetime and high structural stability. In particular, modification of the cyclometalating ligand (C^N ligand) can control the emission color throughout the entire visible region that can be beneficial for realizing full-color and white-light displays. However, deep red phosphorescence with good color purity has been difficult to achieve due to a very wide full width at half maximum (FWHM) for most iridium(III) complexes.[28,29] To design a novel family of color-tunable efficient phosphorescent materials, we have been interested in B- or N-embedded dioxygen-bridged polycyclic units with good rigidity, and electron-withdrawing or electron-donating features that may help reduce the barrier height for electron or hole injection.

In addition, tricoordinate boron-containing units possess certain Lewis acidity and can react with Lewis bases to form the corresponding tetracoordinate adducts,[5,7,30–34] which could induce new electronic and optical properties. However, most studies on planar tricoordinate boron-containing compounds

[a]*School of Material Science and Engineering, Jiangsu University of Science and Technology, Zhenjiang 212003, P. R. China. E-mail: shichao@just.edu.cn; aihua.yuan@just.edu.cn*

[b]*School of Environmental and Chemical Engineering, Jiangsu University of Science and Technology, Zhenjiang 212003, P. R. China*

[c]*Department of Chemistry, Hubei Key Lab on Organic and Polymeric Optoelectronic Materials, Wuhan University, Wuhan 430072, P. R. China. E-mail: clyang@whu.edu.cn*

[d]*State Key Laboratory of Coordination Chemistry, Nanjing University, Nanjing 210093, P. R. China. E-mail: hyan1965@nju.edu.cn*

† Electronic supplementary information (ESI) available. CCDC 1832468–1832470 and 1860052–1860055. For ESI and crystallographic data in CIF or other electronic format see DOI: 10.1039/c8sc04252g

are mainly focused on pure organic π-conjugated molecules,[1–12] which often show fluorescence rather than phosphorescence. Furthermore, how the structure and electrical properties of Lewis bases affect the excited state energy of the adduct still needs further research. So it is anticipated that introduction of B- and N-embedded dioxygen-bridged polycyclic units into phosphorescent iridium(III) complexes may improve the structure and the optical properties of these complexes and allow better understanding the roles of the units.

Herein, we first designed and synthesized a no-atom embedded phosphorescent iridium(III) complex, Ir-OO, as a model complex (Scheme 1) and then prepared a series of B- and N-embedded phosphorescent iridium(III) complexes, containing single-atom embedded complexes (Ir-ON and Ir-OB) and two-atom embedded complexes (Ir-NN and Ir-BB) (Scheme 1). The results demonstrate that the B-embedded polycyclic unit can exhibit better planarity than the N-embedded polycyclic unit, which leads to different π–π-stacking and electrical characteristics. More importantly, by controlling the number of boron or nitrogen atoms embedded, OLED devices incorporating these emitters as emitting layers can achieve a phosphorescence color variation from green to deep red and show low-efficiency roll-off and turn-on voltage. In particular, the B-embedded complex Ir-BB shows good color purity with a narrow full width at half maximum (1211 cm^{-1}) and CIE coordinates (0.67, 0.31) in the saturated deep red light region. Notably, tricoordinate planar B-embedded complexes can also form their corresponding tetracoordinate B–N Lewis adducts (Ir-OB·L and Ir-BB·L, Scheme 1) with addition of Lewis bases L (pyridine and 4-dimethylaminopyridine (DMAP)). During this process, significantly different structural and optical changes are triggered by the structure and electronic properties of Lewis bases, as confirmed by X-ray crystallographic, ^{1}H NMR and spectral analysis.

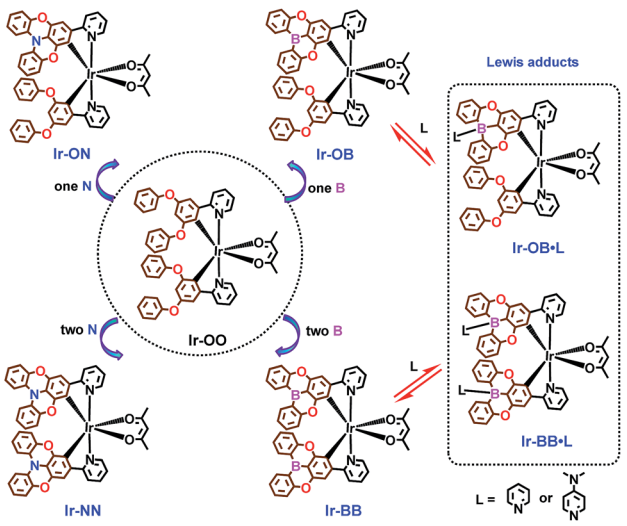

Scheme 1 Chemical structures of B- and N-embedded phosphorescent iridium complexes (Ir-ON, Ir-NN, Ir-OB and Ir-BB) and the model complex Ir-OO, and the conversion from tricoordinate B-embedded complexes (Ir-OB and Ir-BB) to their corresponding tetracoordinate Lewis adducts (Ir-OB·L and Ir-BB·L) in the presence of Lewis base L.

Results and discussion

Synthesis and structure

A ligand (L-1) without atom-embedment was gained by reaction of 2-(3,5-difluorophenyl)pyridine and phenol with excess base. The N-embedded ligand (L-2) was finally prepared through an efficient Suzuki–Miyaura cross-coupling reaction by using N-embedded polycyclic unit-based boron ester as a boron reagent, while the B-embedded ligand (L-3) was synthesized by a one-step debromoborylation reaction of 2-(4-bromo-3,5-diphenoxyphenyl)pyridine (Fig. S1†). Then, all complexes can be prepared according to well-established methods[35–37] for the synthesis of the traditional complex [Ir(C^N)$_2$(acac)] by adding two same (for Ir-NN and Ir-BB) or different (for Ir-ON and Ir-OB) C^N ligands (Fig. S2†). All the new iridium(III) complexes were completely identified by ^{1}H NMR, ^{13}C NMR, HR-MS, elemental analysis and single-crystal X-ray crystallography. All the crystal structures (Fig. 1, and S4–S8, and Table S1†) show that the iridium center can be coordinated by two same (for Ir-NN, Ir-BB and Ir-OO) or different (for Ir-ON and Ir-OB) C^N ligands and one acetylacetone anion ligand in a distorted octahedral coordination geometry. Notably, the B-embedded dioxygen-bridged polycyclic unit in the crystal structure Ir-BB or Ir-OB shows higher planarity with smaller torsion angles (Ir-OB: 0.127° and −2.586°, Ir-BB: 0.024° and −4.044°) (Fig. 1) than (Ir-ON: 21.030° and 31.125°, Ir-NN: 22.691° and 14.953°) (Fig. 1) the N-embedded dioxygen-bridged polycyclic unit in the crystal structure Ir-ON or Ir-NN, and even higher than (18.9°) a B-embedded dioxygen-bridged polycyclic unit-based helical structure reported by the Hatakeyama group.[15] Another

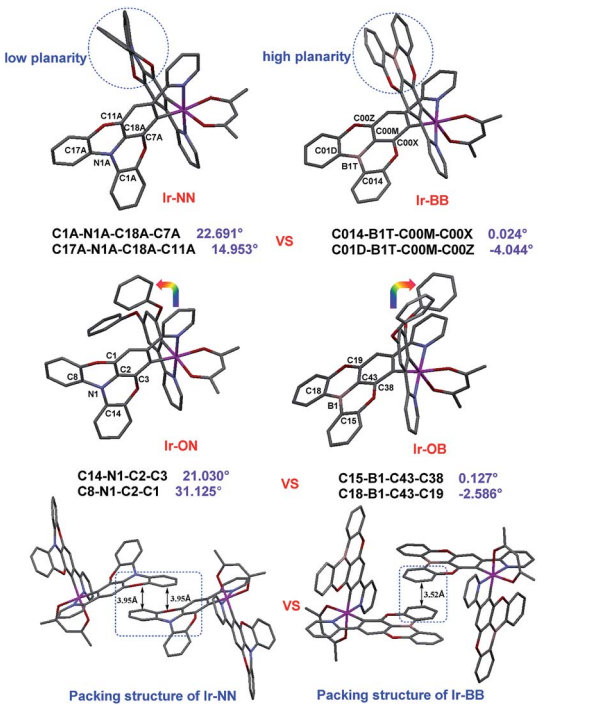

Fig. 1 The X-ray crystal structures of Ir-ON, Ir-NN, Ir-OB and Ir-BB and the packing diagram of Ir-NN and Ir-BB.

interesting structural feature is the packing style of Ir-NN and Ir-BB (Fig. 1). Ir-NN shows a larger overlapping area of π–π-stacking relative to Ir-BB, and the intermolecular distance (3.95 Å) of Ir-NN is longer than that of Ir-BB (3.52 Å). In contrast, Ir-OB, Ir-ON and Ir-OO show little π–π-stacking (Fig. S4–S6†) owing to the distorted structure of the 3,5-diphenoxybenzene unit, which can cause greater steric hindrance than B- or N-embedded planar dioxygen-bridged polycyclic units. Unexpectedly, the orientations of the two phenoxy groups are completely opposite between Ir-ON and Ir-OB (Fig. 1).

Photophysical and electrochemical properties

As shown in Fig. 2a and S3,† according to the UV/visible absorption spectra of all iridium complexes (Ir-OO, Ir-ON, Ir-OB, Ir-NN and Ir-BB) and the corresponding ligands (L-1, L-2 and L-3) in degassed CH_2Cl_2, it is found that the intense absorption bands below 340 nm can be assigned to the spin-allowed π → π* (LC) transitions of the C^N ligands. The weak low-energy absorption band in the region of 350–560 nm is assigned to various charge-transfer (CT) transitions (MLCT, LLCT or ILCT). Notably, the lowest energy bands of B-embedded iridium(III) complexes (Ir-OB and Ir-BB) are clearly red-shifted relative to those of N-embedded iridium(III) complexes (Ir-ON and Ir-NN) – that is, introduction of boron atoms can greatly lower the excited-state energy level. A similar change trend is also found in their PL spectra in CH_2Cl_2. The phosphorescence color can be tuned from green (Ir-OO, 544 nm) to deep red (Ir-BB, 638 nm) by embedding two boron atoms, and the red shift range is nearly 100 nm. In addition, the B-embedded iridium(III) complexes (Ir-OB: Φ_{PL} = 31%, τ = 1.6 μs; Ir-BB: Φ_{PL} = 21%, τ = 1.4 μs) show higher phosphorescence efficiencies and longer emission lifetimes (Table 1) than N-embedded iridium(III) complexes (Ir-ON: Φ_{PL} = 18%, τ = 1.2 μs; Ir-NN: Φ_{PL} = 11%, τ = 1.2 μs) in CH_2Cl_2. In contrast, in CBP: m-MTDATA mixed films, B-embedded iridium(III) complexes (Ir-OB: Φ_{PL} = 44%, τ = 8.4 μs; Ir-BB: Φ_{PL} = 34%, τ = 7.3 μs) exhibit lower phosphorescence efficiencies and shorter emission lifetimes (Table 1) than N-embedded iridium(III) complexes (Ir-ON: Φ_{PL} = 53%, τ = 13 μs; Ir-NN: Φ_{PL} = 50%, τ = 15 μs). The electrochemical properties of all complexes were studied by cyclic voltammetry in CH_2Cl_2 (Fig. S10† and Table 1). The oxidation potentials of the iridium center for all B- and N-embedded iridium(III) complexes (Ir-ON: 0.64 V, Ir-NN: 0.93 V, Ir-OB: 0.99 V and Ir-BB: 0.95 V) show an obvious redshift than that of Ir-OO (0.35 V). In addition, the oxidation potentials of B-embedded polycyclic units (Ir-OB: 0.31 V and Ir-BB: 0.28 V) exhibit a small redshift relative to that of the N-embedded polycyclic unit (Ir-ON: 0.21 V and Ir-NN: 0.22 V). Therefore, introduction of boron and nitrogen atoms can greatly increase the HOMO energy level, especially for complexes Ir-ON (HOMO value: −5.01 eV) and Ir-NN (HOMO value: −5.02 eV), which show HOMO values about 0.13 eV more than that of Ir-OO (HOMO value: −5.15 V).

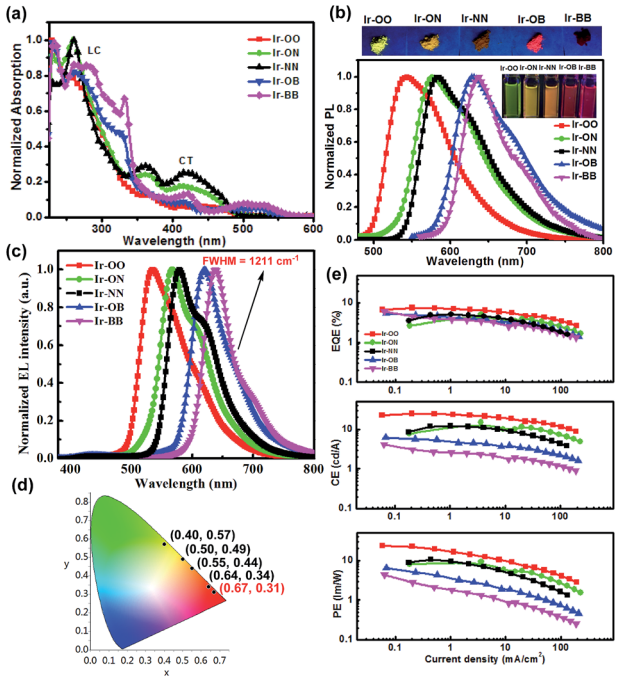

Fig. 2 (a) Absorption and (b) PL spectra of Ir-OO, Ir-ON, Ir-NN, Ir-OB and Ir-BB in degassed CH_2Cl_2 (inset: luminescence photographs of iridium complexes). (c) EL spectra and (d) CIE coordinates and (e) the efficiency *versus* current density relationship for devices of all complexes.

Solution-processed OLED device characterization

All iridium(III) complexes were tested in unoptimized solution-processed OLED devices with the same simple architecture of ITO/PEDOT: PSS (50 nm)/CBP (45%): m-MTDATA (45%): Ir complex (10%) (60 nm)/DPEPO (10 nm)/TmPyPB (50 nm)/Liq (1 nm)/Al (100 nm) (Fig. 2, S11, and S12, and Table S3†). Electroluminescence spectra (538–638 nm) (Fig. 2c) of all complexes resemble their PL spectra measured in CH_2Cl_2 (Fig. 2b). Notably, Ir-BB shows deep red (638 nm) emission, which is more red shifted than the non-embedded boron complex Ir(ppy-$B(Mes)_2)_2$acac (609 nm) reported by the Wong group.[28] Furthermore, it also shows good color purity with CIE coordinates (0.67, 0.31) in the saturated deep red light region and a narrow FWHM (1211 cm^{-1}) (Fig. 2c and d) and is superior to other iridium complexes reported.[28,29] In addition, all complex-based devices show low-efficiency roll-off (Fig. 2e) and turn-on voltage (2.9–3.4 V) (Table S3†). This can be attributed to B- or N-embedded polycyclic units which can reduce the barrier for electron or hole injection. Nevertheless, they all display relatively lower maximum external quantum efficiencies (EQEs) (5.1–7.5%) than other excellent iridium[38–41] and platinum[42] complexes, and thermally activated delayed fluorescent (TADF) materials[43–50] reported in the orange–red region (EQE > 10%). The relatively poor device performance is most likely due to the undesirable solubility of these iridium complexes in the solution process.

B–N Lewis adducts

To investigate the Lewis acidity of B-embedded iridium(III) complexes (Ir-OB and Ir-BB), we choose two different Lewis

Table 1 Photophysical data of Ir(III) complexes

Complexes	λ_{abs} nm (log ε)	PL[a]/PL[c] (nm)	$E_{1/2}^{ox}$ (V)	E_g[b] (eV)	HOMO/LUMO[b] (eV)	Φ_{PL}[a]/Φ_{PL}[c] (%)	τ[a]/τ[c] (μs)
Ir-OO	231 (5.20), 259 (5.11), 366 (4.24), 429 (3.87), 484 (3.36), 497 (2.94)	544/538	0.35	2.40	−5.15/−2.75	15/68	1.1/5.6
Ir-ON	230 (5.24), 259 (5.29), 364 (4.66), 419 (4.51), 481 (3.84), 512 (2.45)	577/568	0.21/0.64	2.36	−5.01/−2.65	18/53	1.2/13
Ir-NN	230 (5.47), 259 (5.58), 363 (4.98), 419 (4.91), 486 (3.93), 516 (2.52)	583/579	0.22/0.34/0.93	2.33	−5.02/−2.69	11/50	1.2/15
Ir-OB	231 (5.20), 260 (5.11), 327 (4.87), 416 (4.08), 523 (3.84), 559 (2.49)	630/622	0.31/0.99	2.21	−5.11/−2.90	31/44	1.6/8.4
Ir-BB	233 (5.28), 262 (5.21), 332 (5.11), 422 (4.36), 499 (4.11), 560 (3.38)	638/639	0.28/0.95	2.15	−5.08/−2.93	21/34	1.4/7.3

[a] Recorded in degassed CH_2Cl_2 at a concentration of 10^{-5} M at 298 K with an excitation wavelength of 370 nm. [b] The HOMO (eV) = $-e(E_{1/2}^{ox} + 4.8)$ and $E_g = 1240/\lambda$, where λ is the absorption wavelength threshold. LUMO (eV) = E_g + HOMO. [c] Measured for 10 wt% doped CBP: m-MTDATA mixed films.

bases (pyridine and DMAP) for comparison. Fortunately, single crystals of the B–N Lewis adducts Ir-BB·pyridine and Ir-BB·DMAP were obtained (Fig. 3 and S9, and Table S2†). It is found that the original planar B-embedded polycyclic units have formed shallow bowl-shaped structures (Fig. 3) due to B–N coordination. Interestingly, as Ir-BB has two boron-containing planes, two Lewis base molecules have different coordination modes: firstly, only one base molecule coordinates at the angle between the two planes (Fig. 3a), and the other base molecule binds on the outside of one plane (Fig. 3a, mode 1), such as in Ir-BB·pyridine (Fig. 3b). Secondly, these two base molecules both bind at the angle between the two planes (Fig. 3d, mode 2), such as in Ir-BB·DMAP (Fig. 3e). Unexpectedly, the obvious π–π interaction between two pyridine moieties (the distance is 3.42 Å) can be observed in the crystal structure of Ir-BB·DMAP (Fig. 3e), but not in the crystal structure of Ir-BB·pyridine (Fig. 3b) due to different coordination modes. It is notable that the B–N distance of Ir-BB·DMAP(1.638 Å and 1.672 Å) is shorter than that of Ir-BB·pyridine (1.658 Å and 1.688 Å) (Fig. 3b and e). This comparison demonstrates a rather stronger B–N coordination in Ir-BB·DMAP due to the higher Lewis basicity of DMAP relative to pyridine. Such interesting structural changes can also be monitored by ^{1}H NMR spectroscopy in d_6-DMSO solution. With addition of excess pyridine (41 eq.) and DMAP (10 eq.), all the original nuclear magnetic peaks of Ir-BB disappear and some new peaks emerge, which are assigned to Ir-BB·pyridine (Fig. 3c) and Ir-BB·DMAP (Fig. 3f), respectively.

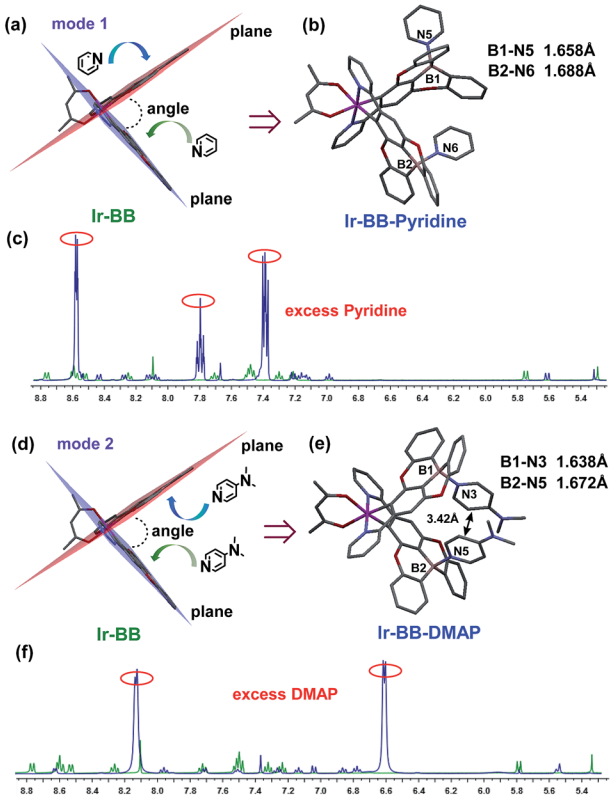

Fig. 3 The X-ray crystal structures of (b) Ir-BB·pyridine and (e) Ir-BB·DMAP were formed through the coordination of Ir-BB and two pyridine molecules by mode 1 (a) and two DMAP molecules by mode 2 (d), respectively. Titrations of Ir-BB in d_6-DMSO with excess pyridine (c) and DMAP (f) monitored by ^{1}H NMR spectroscopy.

Additionally, the optical changes caused by the newly formed B–N Lewis adducts can be monitored by UV and PL titration experiments (Fig. 4). Upon addition of pyridine or DMAP, all the absorption bands (LC and CT) of Ir-BB are gradually decreased (Fig. 4a and b), which should be attributed to the fact that the newly formed tetracoordinate borides break the π-conjugation of the ligand, thereby weakening the UV absorption. Interestingly, with addition of pyridine, the absorption bands (CT) show a small red shift (Fig. 4a) in contrast to a significant blue shift (Fig. 4b) in the presence of DMAP. A similar change trend is also found in the PL spectrum. The emission peak of Ir-BB is gradually decreased and redshifted from 647 nm to 667 nm (Fig. 4c) with the addition of pyridine, and its phosphorescence lifetime is also changed from 873 ns to 677 ns. In contrast, a significant blue-shift emission peak of Ir-BB·DMAP appears at 575 nm (Fig. 4d) with a shorter phosphorescence lifetime of 183 ns with the addition of DMAP. This comparison indicates that the structure and electronic properties of Lewis bases can affect the excited state energy of the adducts.

In addition, Ir-OB displays a similar structural and optical change in the presence of Lewis bases (Fig. S13 and S14†). The binding constants of Ir-OB toward pyridine and DMAP (DMSO) are estimated to be 19.6 M^{-1} and 8.0 × 10^3 M^{-1} (Fig. S15 and

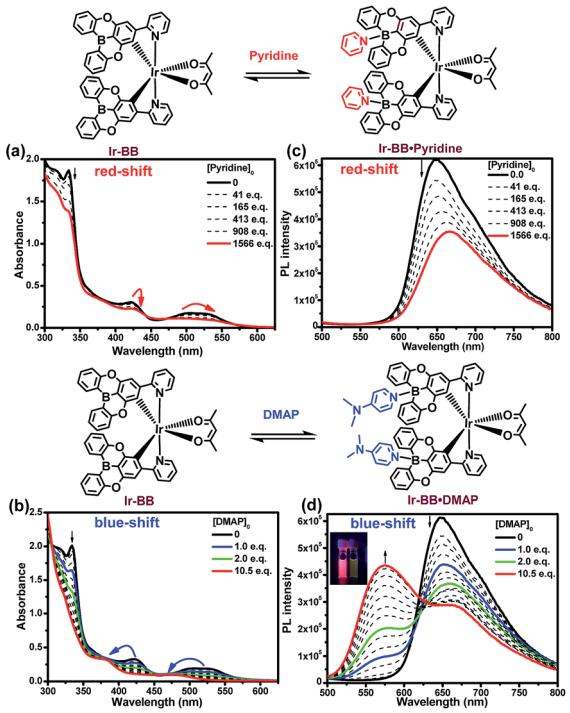

Fig. 4 Titrations of Ir-BB in DMSO ($[Ir\text{-}BB]_0 = 3 \times 10^{-5}$ M) with pyridine (a and c) and DMAP (b and d) monitored by UV-vis absorption (a and b) and phosphorescence ($\lambda_{ex} = 370$ nm) spectroscopy (c and d).

S16†), respectively. These values are much lower than those of trinaphthylborane (5.1×10^3 M^{-1} for pyridine and 6.6×10^6 M^{-1} for DMAP) reported by the Yamaguchi group.[7] The lower Lewis acidity of Ir-OB should be attributed to the larger steric hindrance.

Theoretical calculations

To understand the roles of B- and N-embedded polycyclic units and how the addition of these two Lewis bases affects the excited state behavior of B–N Lewis adducts, DFT calculations at the B3LYP/6-31G(d) level were performed with all the complexes discussed above (Fig. 5, and S17–S19, and Tables S4 and S5†). The HOMOs of the triplet excited state (T_1) of Ir-OO, Ir-OB and Ir-BB are mainly distributed on the iridium(III) center, phenyl ring and two oxygen atoms of the C^N ligand, whereas the HOMOs of Ir-ON and Ir-NN are mainly located on the whole N-embedded C^N ligand but little on the metal iridium (Fig. S17†). The LUMOs of Ir-OO, Ir-OB and Ir-BB are distributed on the whole C^N ligand, and the LUMOs of Ir-ON and Ir-NN reside on 2-phenyl pyridine and the embedded nitrogen atom of the C^N ligand. As a result, the transition character between B and N-embedded complexes is quite different: the transitions of N-embedded iridium(III) complexes exhibit only ^{3}ILCT (for Ir-NN) or ^{3}ILCT and ^{3}LLCT (for Ir-ON) but little ^{3}MLCT, because the charges on the metal iridium cannot be easily transferred to the N-embedded C^N ligand with rich charges. In contrast, the transition of B-embedded iridium(III) complexes do not only show ^{3}ILCT (for Ir-BB) or ^{3}ILCT and ^{3}LLCT (for Ir-OB) but also show ^{3}MLCT (Fig. S17†), which can be attributed to the electron-withdrawing ability of the B-embedded C^N ligand that can easily induce the charge transfer from the metal to the ligand.

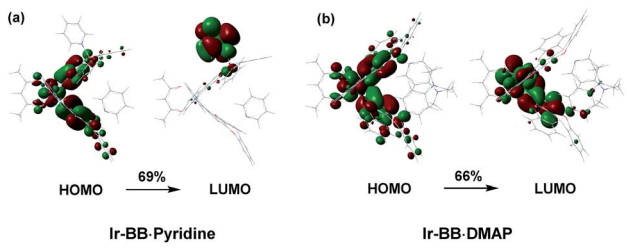

Fig. 5 The optimized geometries and main orbital transitions of (a) Ir-BB·pyridine and (b) Ir-BB·DMAP in the lowest triplet excited state (T_1).

For B–N Lewis adducts, taking Ir-BB·pyridine and Ir-BB·DMAP as an example, the T_1 of two adducts are both dominated by the HOMO → LUMO transition (Fig. 5 and Table S5†). The HOMOs of these two adducts are similar and mainly reside on the iridium(III) center, phenyl ring and two oxygen atoms of the C^N ligand. Interestingly, the LUMO of Ir-BB·DMAP resides on the partial C^N ligand moieties (Fig. 5b), whereas the LUMO of Ir-BB·pyridine is completely located on the Lewis base pyridine moieties (Fig. 5a). As a result, Ir-BB·DMAP has MLCT transition character in T_1, while the T_1 of Ir-BB·pyridine exhibits intramolecular charge transfer character from the Lewis acid Ir-BB to Lewis base pyridine. This result can explain the above significantly different optical changes triggered by the structure and electronic properties of Lewis bases.

Conclusions

In conclusion, we have prepared a novel family of B- and N-embedded phosphorescent iridium(III) complexes. By controlling the number of boron or nitrogen atoms embedded, OLED devices incorporating these emitters as emitting layers can lead to a phosphorescence color change from green to deep red. In particular, the B-embedded complex Ir-BB shows good color purity with a narrow full width at half maximum (1211 cm^{-1}) and CIE coordinates (0.67, 0.31) in the saturated deep red light region. We also investigate B-embedded complex-based B–N Lewis adducts containing different Lewis bases and understand the correlations between the intriguing structure and optical properties. This work provides a new strategy for the investigation and application of B- and N-embedded phosphorescent materials and also extends the scope of B- and N-embedded semiconductors from pure organic molecules to metal complexes.

Conflicts of interest

There are no conflicts to declare.

Acknowledgements

This work was supported by the National Natural Science Foundation of China (21601069, 51672114, 21531004 and

91433201), Natural Science Foundation of Jiangsu Province of China (BK20160552 and BK20161357), Natural Science Foundation of the Higher Education Institutions of Jiangsu Province (16KJB150011), Postdoctoral Research Foundation of China (2017M611746) and Jiangsu Postdoctoral Research Foundation (1701115B).

Notes and references

1 S. Nakatsuka, H. Gotoh, K. Kinoshita, N. Yasuda and T. Hatakeyama, *Angew. Chem., Int. Ed.*, 2017, **56**, 5087.
2 Z. X. Giustra and S.-Y. Liu, *J. Am. Chem. Soc.*, 2018, **140**, 1184.
3 X.-Y. Wang, F.-D. Zhuang, R.-B. Wang, X.-C. Wang, X.-Y. Cao, J.-Y. Wang and J. Pei, *J. Am. Chem. Soc.*, 2014, **136**, 3764.
4 X.-Y. Wang, H.-R. Lin, T. Lei, D.-C. Yang, F.-D. Zhuang, J.-Y. Wang, S.-C. Yuan and J. Pei, *Angew. Chem., Int. Ed.*, 2013, **52**, 3117.
5 S. Saito, K. Matsuo and S. Yamaguchi, *J. Am. Chem. Soc.*, 2012, **134**, 9130.
6 K. Matsuo, S. Saito and S. Yamaguchi, *Angew. Chem., Int. Ed.*, 2016, **55**, 1.
7 K. Matsuo, S. Saito and S. Yamaguchi, *J. Am. Chem. Soc.*, 2014, **136**, 12580.
8 T. Hatakeyama, S. Hashimoto, S. Seki and M. Nakamura, *J. Am. Chem. Soc.*, 2011, **133**, 18614.
9 T. Hatakeyama, S. Hashimoto, T. Oba and M. Nakamura, *J. Am. Chem. Soc.*, 2012, **134**, 19600.
10 T. Hashimoto, T. Ikuta, K. Shiren, S. Nakatsuka, J. Ni, M. Nakamura and T. Hatakeyama, *Chem. Mater.*, 2014, **26**, 6265.
11 C. Dou, S. Saito, K. Matsuo, I. Hisaki and S. Yamaguchi, *Angew. Chem., Int. Ed.*, 2012, **51**, 12206.
12 Z. Zhou, A. Wakamiya, T. Kushida and S. Yamaguchi, *J. Am. Chem. Soc.*, 2012, **134**, 4529.
13 K. Suzuki, S. Kubo, K. Shizu, T. Fukushima, A. Atsushi-Wakamiya, Y. Murata, C. Adachi and H. Kaji, *Angew. Chem., Int. Ed.*, 2015, **54**, 15231.
14 W. Zhang, G. Li, L. Xu, Y. Zhuo, W. Wan, N. Yan and G. He, *Chem. Sci.*, 2018, **9**, 4444.
15 K. Hirai, K. Nakajima, S. Nakatsuka, K. Shiren, J. Ni, S. Nomura, T. Ikuta and T. Hatakeyama, *Angew. Chem., Int. Ed.*, 2015, **54**, 13581.
16 A. Wakamiya, H. Nishimura, T. Fukushima, F. Suzuki, A. Saeki, S. Seki, I. Osaka, T. Sasamori, M. Murata, Y. Murata and H. Kaji, *Angew. Chem., Int. Ed.*, 2014, **53**, 5800.
17 M. A. Baldo, M. E. Thompson and S. R. Forrest, *Nature*, 2000, **403**, 750.
18 A. Tsuboyama, H. Iwawaki, M. Furugori, T. Mukaide, J. Kamatani, S. Igawa, T. Moriyama, T. Miura, T. Takiguchi, S. Okada, M. Hoshino and K. Ueno, *J. Am. Chem. Soc.*, 2003, **125**, 12971.
19 C. Shi, H. Sun, X. Tang, W. Lv, H. Yan, Q. Zhao, J. Wang and W. Huang, *Angew. Chem., Int. Ed.*, 2013, **52**, 13434.
20 K.-H. Kim, S. Lee, C.-K. Moon, S.-Y. Kim, Y.-S. Park, J.-H. Lee, J. W. Lee, J. Huh, Y. You and J.-J. Kim, *Nat. Commun.*, 2014, **5**, 4769.
21 K. Y. Zhang, Q. Yu, H. Wei, S. Liu, Q. Zhao and W. Huang, *Chem. Rev.*, 2018, **118**, 1770.
22 S. Kesarkar, W. Mróz, M. Penconi, M. Pasini, S. Destri, M. Cazzaniga, D. Ceresoli, P. R. Mussini, C. Baldoli, U. Giovanella and A. Bossi, *Angew. Chem., Int. Ed.*, 2016, **55**, 2714.
23 M. J. Jurow, C. Mayr, T. D. Schmidt, T. Lampe, P. I. Djurovich, W. Brütting and M. E. Thompson, *Nat. Mater.*, 2016, **15**, 85.
24 J. Lee, H.-F. Chen, T. Batagoda, C. Coburn, P. I. Djurovich, M. E. Thompson and S. R. Forrest, *Nat. Mater.*, 2016, **15**, 92.
25 P.-N. Lai, C. H. Brysacz, M. K. Alam, N. A. Ayoub, T. G. Gray, J. Bao and T. S. Teets, *J. Am. Chem. Soc.*, 2018, **140**, 10198.
26 X. Li, J. Zhang, Z. Zhao, L. Wang, H. Yang, Q. Chang, N. Jiang, Z. Liu, Z. Bian, W. Liu, Z. Lu and C. Huang, *Adv. Mater.*, 2018, **30**, 1705005.
27 C. Shi, H. Sun, Q. Jiang, Q. Zhao, J. Wang, W. Huang and H. Yan, *Chem. Commun.*, 2013, **49**, 4746.
28 B. G. Zhou, C.-L. Ho, W.-Y. Wong, Q. Wang, D. Ma, L. Wang, Z. Lin, T. B. Marder and A. Beeby, *Adv. Funct. Mater.*, 2008, **18**, 499.
29 P. Tao, W.-L. Li, J. Zhang, S. Guo, Q. Zhao, H. Wang, B. Wei, S.-J. Liu, X.-H. Zhou, Q. Yu, B.-S. Xu and W. Huang, *Adv. Funct. Mater.*, 2016, **26**, 881.
30 K. Ansorg, H. Braunschweig, C.-W. Chiu, B. Engels, D. Gamon, M. Hgüel, T. Kupfer and K. Radacki, *Angew. Chem., Int. Ed.*, 2011, **50**, 2833.
31 D. Frath, J. Massue, G. Ulrich and R. Ziessel, *Angew. Chem., Int. Ed.*, 2014, **53**, 2290.
32 Y.-J. Shiu, Y.-C. Cheng, W.-L. Tsai, C.-C. Wu, C.-T. Chao, W. Lu, Y. Chi, Y.-T. Chen, S.-H. Liu and P.-T. Chou, *Angew. Chem., Int. Ed.*, 2016, **55**, 3017.
33 S. Osumi, S. Saito, C. Dou, K. i. Matsuo, K. Kume, H. Yoshikawa, K. Awagaa and S. Yamaguchi, *Chem. Sci.*, 2016, **7**, 219.
34 K. Liu, R. A. Lalancette and F. Jäkle, *J. Am. Chem. Soc.*, 2017, **139**, 18170.
35 S. Lamansky, P. Djurovich, D. Murphy, F. Abdel-Razzaq, H.-E. Lee, C. Adachi, P. E. Burrows, S. R. Forrest and M. E. Thompson, *J. Am. Chem. Soc.*, 2001, **123**, 4304.
36 X. Xu, X. Yang, J. Dang, G. Zhou, Y. Wu, H. Li and W.-Y. Wong, *Chem. Commun.*, 2014, **50**, 2473.
37 X. Xu, H. Guo, J. Zhao, B. Liu, X. Yang, G. Zhou and Z. Wu, *Chem. Mater.*, 2016, **28**, 8556.
38 R. Wang, D. Liu, H. Ren, T. Zhang, H. Yin, G. Liu and J. Li, *Adv. Mater.*, 2011, **23**, 2823.
39 Y. Zheng, A. S. Batsanov, M. A. Fox, H. A. Al-Attar, K. Abdullah, V. Jankus, M. R. Bryce and A. P. Monkman, *Angew. Chem., Int. Ed.*, 2014, **53**, 11616.
40 Z. Chen, L. Wang, C.-L. Ho, S. Chen, S. Suramitr, A. Plucksacholatarn, N. Zhu, S. Hannongbua and W.-Y. Wong, *Adv. Opt. Mater.*, 2018, **6**, 1800824.
41 B. Jiang, C. Zhao, X. Ning, C. Zhong, D. Ma and C. Yang, *Adv. Opt. Mater.*, 2018, **6**, 1800108.
42 G. Cheng, Q. Wan, W.-H. Ang, C.-L. Kwong, W.-P. To, P.-K. Chow, C.-C. Kwok and C.-M. Che, *Adv. Opt. Mater.*, 2018, DOI: 10.1002/adom.201801452.

43 W. Zeng, H.-Y. Lai, W.-K. Lee, M. Jiao, Y.-J. Shiu, C. Zhong, S. Gong, T. Zhou, G. Xie, M. Sarma, K.-T. Wong, C.-C. Wu and C. Yang, *Adv. Mater.*, 2018, **30**, 1704961.
44 K. Wu, T. Zhang, Z. Wang, L. Wang, L. Zhan, S. Gong, C. Zhong, Z.-H. Lu, S. Zhang and C. Yang, *J. Am. Chem. Soc.*, 2018, **140**, 8877.
45 C. Chen, R. Huang, A. S. Batsanov, P. Pander, Y.-T. Hsu, Z. Chi, F. B. Dias and M. R. Bryce, *Angew. Chem., Int. Ed.*, 2018, **57**, 16407.
46 C. Li, R. Duan, B. Liang, G. Han, S. Wang, K. Ye, Y. Liu, Y. Yi and Y. Wang, *Angew. Chem., Int. Ed.*, 2017, **56**, 11525.
47 H. Wang, L. Meng, X. Shen, X. Wei, X. Zheng, X. Lv, Y. Yi, Y. Wang and P. Wang, *Adv. Mater.*, 2015, **27**, 4041.
48 S. Y. Lee, T. Yasuda, Y. S. Yang, Q. Zhang and C. Adachi, *Angew. Chem., Int. Ed.*, 2014, **53**, 6402.
49 Q. Zhang, H. Kuwabara, W. J. P. Jr, S. Huang, Y. Hatae, T. Shibata and C. Adachi, *J. Am. Chem. Soc.*, 2014, **136**, 18070.
50 D.-H. Kim, A. D'Aléo, X.-K. Chen, A. D. S. Sandanayaka, D. Yao, L. Zhao, T. Komino, E. Zaborova, G. Canard, Y. Tsuchiya, E. Choi, J. W. Wu, F. Fages, J.-L. Brédas, J.-C. Ribierre and C. Adachi, *Nat. Photonics*, 2018, **12**, 98.